Dynamics-dependent synchronization in on-chip coupled semiconductor lasers

Shoma Ohara,[1,*] Andreas Karsaklian Dal Bosco,[1,†] Kazusa Ugajin,[1] Atsushi Uchida,[1,‡]
Takahisa Harayama,[2] and Masanobu Inubushi[3]

[1]*Department of Information and Computer Sciences, Saitama University, 255 Shimo-Okubo Sakura-ku, Saitama City, Saitama 338-8570, Japan*

[2]*Department of Applied Physics, School of Advanced Science and Engineering, Faculty of Science and Engineering, Waseda University 3-4-1 Okubo, Shinjuku-ku, Tokyo 169-8555, Japan*

[3]*NTT Communication Science Laboratories, NTT Corporation, 3-1 Morinosato, Wakamiya, Atsugi-Shi, Kanagawa 243-0198, Japan*

(Received 21 April 2017; published 18 September 2017)

Synchronization properties of chaotic dynamics in two mutually coupled semiconductor lasers with optical feedback embedded in a photonic integrated circuit are investigated from the point of view of their dynamical content. A phenomenon in which the two lasers can show qualitatively different synchronization properties according to the frequency range of investigation and their nonlinear dynamics is identified and termed dynamics-dependent synchronization. In-phase synchronization is observed for original signals and antiphase synchronization is observed for low-pass filtered signals in the case where one of the lasers shows chaotic oscillations while the other laser exhibits low-frequency fluctuations dynamics. The experimental conditions causing the synchronization states to vary according to the considered frequency interval are studied and the key roles of asymmetric coupling strength and injection currents are clarified.

DOI: 10.1103/PhysRevE.96.032216

I. INTRODUCTION

Coupled nonlinear systems show a variety of dynamical behavior. Recently, chaos synchronization in coupled semiconductor lasers has been widely reported for understanding fundamental physics, as well as for information security applications in chaos-based optical-communication schemes [1–3] and secure key distribution [4–6]. For example, isochronal (zero-lag) synchronization and cluster synchronization have been proposed when chaotic lasers are coupled, and globally coupled laser networks have been studied for neuromorphic information processing [9–15].

Low-frequency fluctuations (LFF) has been reported as one of the dominant nonlinear dynamical phenomena in semiconductor lasers with optical self-feedback [7,8]. LFF dynamics consists of high-frequency chaotic oscillations and low-frequency sudden power dropouts [16–20]. Synchronization of LFF dynamics has been observed in the chaotic output of two mutually coupled lasers with the peak frequency corresponding to the inverse of twice the coupling time delay [21]. The two chaotic temporal waveforms are synchronized with the time lag of the coupling delay time. This is known as the leader-laggard relationship, in which spontaneous symmetry-breaking occurs, even though lasers are coupled symmetrically [21,22]. In addition, antiphase synchronization of LFF dynamics has been observed in mutually coupled semiconductor lasers [23]. Episodic synchronization has also been reported when the optical frequency detuning between the coupled lasers fluctuates in time [24,25].

Parameter mismatch in coupled laser systems has a strong impact on both their nonlinear dynamics and synchronization state. In Ref. [26], it has been reported that the mismatch of self- and cross-coupling strengths affects the stability of the zero-lag synchronization state but keeps the dynamics unchanged. However, the mismatch of self- and cross-coupling delay does not affect the quality of synchronization but alters the dynamics significantly. In Ref. [27], antiphase synchronization and generalized synchronization have been observed by changing one of the parameter values in coupled electro-optic oscillators.

Dynamics and chaos synchronization in mutually coupled semiconductor lasers have been investigated mostly for long external cavity configurations and long coupling delays (>100 mm) in free-space and fiber-based optical systems [7,8,28,29]. The external cavity length is an essential parameter when considering a semiconductor laser with time-delayed optical feedback. Long and short external cavity lengths are defined as $\tau_r < \tau_{\mathrm{ext}}$ and $\tau_r > \tau_{\mathrm{ext}}$, respectively [28], where τ_r is the relaxation oscillation period and τ_{ext} is the round-trip propagation time of light in the external cavity.

Recently, photonic integrated circuits (PICs) have been proposed as monolithically integrated optical systems with short external cavities (∼10 mm) [30]. A variety of nonlinear dynamics has been reported using this kind of PICs, such as fast self-pulsations [31], chaotic oscillations [30], regular pulse packages [32], and intermittency [33]. PICs are also suitable entropy sources for physical random number generation at rates over the GHz order [34–36]. Synchronization has been observed in the particular case of periodic oscillations in a PIC with two semiconductor lasers coupled very closely (0.3 mm) [37]. However, chaos synchronization in a PIC with two mutually coupled semiconductor lasers has not been reported yet. PICs has brought new technological advantages for robust and in-depth investigation of dynamics and chaos synchronization in coupled lasers to avoid phase fluctuation against air turbulence and temperature fluctuations. This major advance motivates in-depth investigations of complex

*s.ohara.836@ms.saitama-u.ac.jp

†Present address: RIKEN Center for Advanced Photonics, RIKEN, Japan.

‡auchida@mail.saitama-u.ac.jp

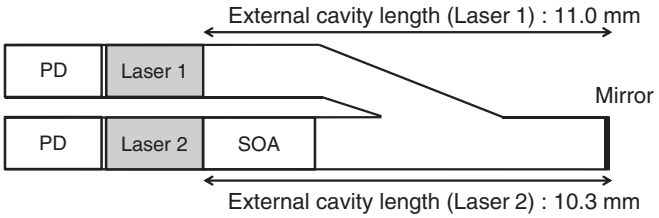

FIG. 1. Schematics of the photonic integrated circuit with two mutually coupled semiconductor lasers. PD, photodiode; Lasers 1 and 2, distributed feedback lasers; SOA, semiconductor optical amplifier.

integrated optical systems such as coupled lasers with reliable reproducibility and stability conditions. In addition, it is important to investigate how the dynamical change affects the state of synchronization in the coupled lasers. However, no comprehensive study on the relationship between the dynamics and synchronization has been reported so far.

In this paper, we demonstrate that two different dynamics of chaos and LFFs can simultaneously induce in-phase and antiphase synchronization on distant frequency ranges, and we term dynamics-dependent synchronization. We fabricate a PIC with two mutually coupled semiconductor lasers with asymmetric optical coupling and feedback to observe the dynamics-dependent synchronization. We experimentally investigate chaos synchronization in the PIC and focus on the dependence of the synchronization quality on different frequency components by using a low-pass filter. We study the influence of the nature of the different dynamics exhibited in each laser on the synchronization state to understand the overall synchronization scenario of the PIC.

II. EXPERIMENTAL SETUP

Our PIC is depicted in Fig. 1. The PIC consists of two distributed feedback (DFB) semiconductor lasers (called laser 1 and laser 2) that are coupled mutually, two photodetectors (PD), a semiconductor optical amplifier (SOA), a passive Y-shaped waveguide, and a common external mirror. The optical outputs from both lasers are reflected back by the external mirror as optical feedback signals. In addition, each laser's output is reflected and injected into the other for mutual coupling. The external mirror provides both feedback and coupling beams to realize a delayed-shared feedback coupling scheme [27]. Chaotic oscillations can be generated due to the nonlinear interaction between the external cavity frequencies defined by the presence of a delayed feedback, the propagation frequency between the coupled lasers, and the relaxation oscillation frequencies of the two lasers.

We fabricated the laser chip with a Y-branch configuration (see Fig. 1), which results in the asymmetric external cavity lengths (one-way) of 11.0 and 10.3 mm for laser 1 and 2, respectively. The corresponding round-trip feedback delay times $\tau_{\mathrm{ext},i}$ for the laser i ($i = 1$ or 2) are 0.29 and 0.27 ns, which are calculated from $\tau_{\mathrm{ext},i} = 2nL_{\mathrm{ext},i}/c$, where $L_{\mathrm{ext},i}$ is the external cavity length (one-way) corresponding to the distance from the laser to the external mirror, $n = 3.9$ is the refractive index of the PIC material, and c is the speed of light in vacuum. The corresponding external cavity frequencies $f_{\mathrm{ext},i} = 1/\tau_{\mathrm{ext},i}$ are 3.4 and 3.7 GHz for laser 1 and 2, respectively. In addition, the one-way coupling delay time between the two lasers is 0.28 ns, obtained from $\tau_c = n(L_{\mathrm{ext},1} + L_{\mathrm{ext},2})/c$. The corresponding coupling frequency $f_c = 1/\tau_c$ is 3.6 GHz.

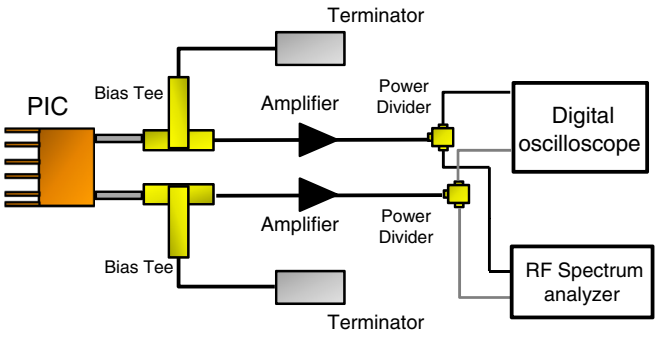

FIG. 2. Scheme of the experimental setup using photonic integrated circuit (PIC).

We cannot measure the relaxation oscillation frequency precisely, since the laser output are too week to measure without optical feedback or coupling. We consider that the relaxation oscillation frequency increases and becomes higher than the external cavity frequencies (3.4 and 3.7 GHz) as the injection currents of the DFB lasers are increased. Therefore, the lasers operate either in the long or the short cavity regime according to their injection currents.

The variable parameters are the injection currents for laser 1, laser 2, and the SOA. The lasing threshold currents in both lasers are 12 mA. The feedback strength for laser 2 and the coupling strength between the two lasers are simultaneously varied by changing the SOA injection current, while the feedback strength for laser 1 is fixed. Therefore, the feedback strengths in laser 1 and 2 are asymmetric. We investigate the nonlinear dynamics and the corresponding synchronization state by changing these parameters.

Our experimental setup is presented in Fig. 2. The output of each laser is converted into an electrical signal by the photodetectors embedded in the PIC. Each electrical signal is separated into direct current (DC) and alternating current (AC) components by a bias tee. The AC component is amplified using an electrical amplifier (1422-LFCNew Focus, 20 GHz bandwidth). The electrical signal is detected by a digital oscilloscope (Tektronix DPO71604B, 16 GHz bandwidth, 50 GigaSample/s) and a RF spectrum analyzer (Agilent N9010A, 26.5 GHz bandwidth) to measure the temporal waveforms and RF spectra of the laser intensities, respectively. No optical output port is implemented in the PIC.

We calculate the cross-correlation value between the temporal waveforms of laser 1 and laser 2 to quantitatively evaluate the synchronization quality. The cross-correlation function is defined as follows:

$$C = \frac{\langle (I_1(t-\tau) - \overline{I}_1)(I_2(t) - \overline{I}_2) \rangle}{\sigma_1 \cdot \sigma_2}, \tag{1}$$

where, $I_1(t)$ and $I_2(t)$ are the output intensities of laser 1 and laser 2, respectively. $\overline{I}_1$ and $\overline{I}_2$ are the mean values of $I_1(t)$ and $I_2(t)$. σ_1 and σ_2 are the standard deviations of $I_1(t)$ and $I_2(t)$, respectively. The bracket $\langle\,\rangle$ represents time averaging. We

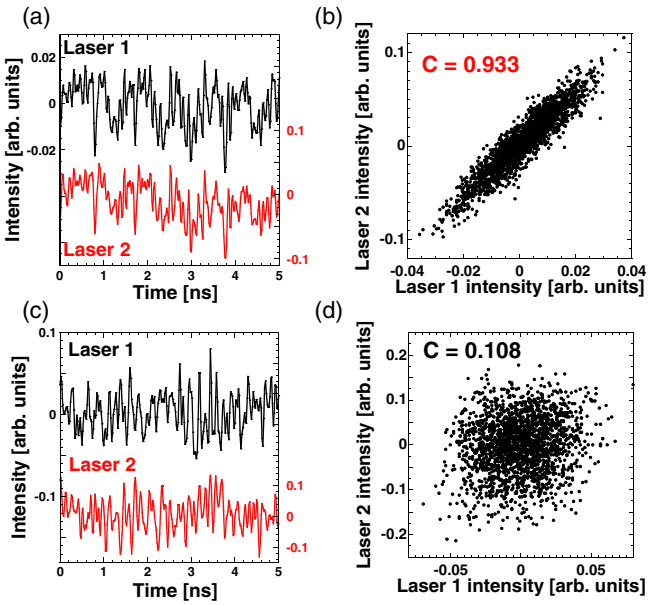

FIG. 3. Experimental observation of chaos synchronization. (a, c) temporal waveforms and (b, d) correlation plots of the two lasers. (a, b) Asymmetric injection currents: $I_1/I_{\mathrm{th},1} = 1.0$, $I_2/I_{\mathrm{th},2} = 4.0$. (c, d) Symmetric injection currents: $I_1/I_{\mathrm{th},1} = 4.0$, $I_2/I_{\mathrm{th},2} = 4.0$. The SOA injection current is fixed at $I_{\mathrm{SOA}} = 15.00$ mA. The cross correlation value is calculated using temporal waveforms recorded on 4 μs. The lag times for which the absolute value of the cross correlation is maximal are (b) -0.42 ns and (d) 0.08 ns.

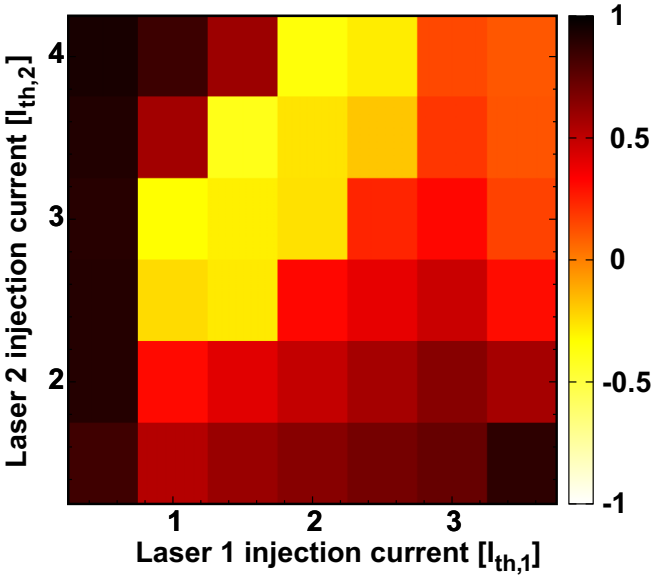

FIG. 4. Two-dimensional diagram of cross-correlation C between the two laser outputs in the PIC. The delay time τ for the calculation of C is adjusted in each case to maximize the absolute value of C. The color scale corresponds to the values of the cross correlation. The normalized injection current for laser 1 ($I_1/I_{\mathrm{th},1}$) is changed from 0.5 to 3.5 with 0.5 interval, and that for laser 2 ($I_2/I_{\mathrm{th},2}$) is changed from 1.5 to 4.0 with 0.5 interval. The SOA injection current is fixed at $I_{\mathrm{SOA}} = 15.00$ mA. Chaos and LFF dynamics are observed in this parameter region.

calculate the maximum absolute value of the cross correlation C by changing the delay time τ continuously.

III. CHAOS SYNCHRONIZATION FOR DIFFERENT INJECTION CURRENTS

Figure 3 shows experimental results of chaos synchronization observed in the PIC. The temporal waveforms of lasers 1 and 2 are shown in Figs. 3(a) and 3(c). The correlation plots between lasers 1 and 2 are shown in Figs. 3(b) and 3(d). $I_i/I_{\mathrm{th},i}$ denotes the injection currents normalized by the lasing threshold, where the index i denotes laser 1 or 2. We set asymmetric and symmetric injection currents in the case of Figs. 3(a) and 3(b) and in the case of Figs. 3(c) and 3(d), respectively. In Figs. 3(a) and 3(b), the values of the injection currents in the lasers are asymmetric and chaos synchronization is observed with the high cross-correlation value of 0.933. By contrast, the two lasers are not synchronized and show the low cross-correlation value of 0.108 when the injection currents are symmetric, as presented in Figs. 3(c) and 3(d). Thus, the cross-correlation value is significantly altered when changing the symmetry in the injection currents between the two lasers. We will discuss the relationship between the change in the dynamics and the degree of synchronization in Sec. IV.

To investigate the conditions of chaos synchronization, we show a two-dimensional cross-correlation diagram in Fig. 4, obtained by making the injection currents in the two lasers vary. When one of the lasers is biased near the lasing threshold, both lasers are well synchronized and high cross-correlation values are obtained. In addition, higher correlation is observed for asymmetric injection currents than for symmetric injection currents. We interpret that a large discrepancy between the injection currents of the lasers results in a large gap in their respective output powers and in the relative coupling beams. In consequence, synchronization phenomena like what can be seen under unidirectional coupling conditions can be easily performed when driving the lasers with asymmetric currents.

IV. FREQUENCY DEPENDENCE OF CHAOS SYNCHRONIZATION

In this section, we address the question of chaos synchronization when the frequency content of the signals changes. We investigate the frequency dependence of chaos synchronization between the original (unfiltered) signals of the two lasers and their low-pass filtered signals when the cut-off frequency of the low-pass filter is set to $f_c = 1$ GHz by using a digital filter. Mainly, we focus on two different dynamics: coherence collapse chaos and LFF. We base the distinction between LFF and chaos on spectral considerations. We consider that the dynamics is LFF when the power of the low-frequency components (<1 GHz) is higher than the power of the chaotic components ($\sim$few GHz) in the RF spectra. Note that the average frequency of the LFF dropouts ranges from tens to hundreds of MHz. We operate in an asymmetric configuration, in which the injection currents are $I_1/I_{\mathrm{th},1} = 1.5$ and $I_2/I_{\mathrm{th},2} = 3.5$.

Figure 5 shows the temporal waveforms and RF spectra of the two lasers when the SOA injection current (I_{SOA}) is changed. We start from a low value of I_{SOA} at 6.00 mA

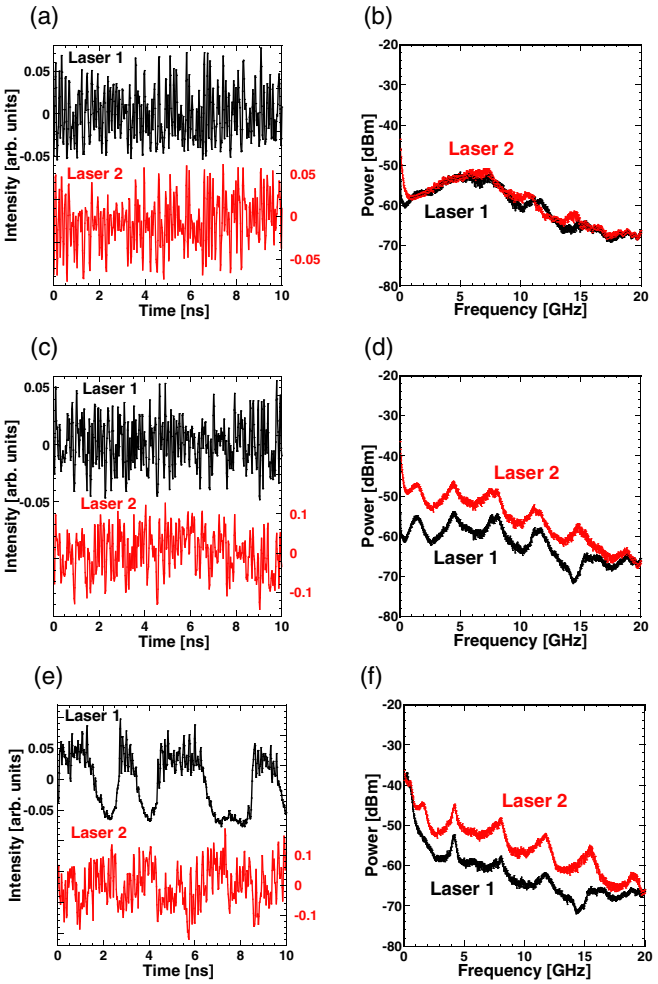

FIG. 5. Dynamics for different SOA injection currents I_{SOA}. (a, c, e) Temporal waveforms and (b, d, f) RF spectra. (a, b) I_{SOA} = 6.00 mA, (c, d) I_{SOA} = 25.00 mA, and (e, f) I_{SOA} = 39.00 mA. The injection currents are $I_1/I_{\mathrm{th},1} = 1.5$ and $I_2/I_{\mathrm{th},2} = 3.5$.

[Figs. 5(a) and 5(b)], for which both lasers exhibit chaos without low-frequency predominance. When I_{SOA} is increased to 25.00 mA [Figs. 5(c) and 5(d)], laser 1 still exhibits chaos, while laser 2 enters a LFF regime, as seen from the gradual increase of low-frequency components in the RF spectrum shown in Fig. 5(d). We interpret that the LFF dynamics in laser 2 is induced by an increase of feedback strength, because the SOA injection current changes both the mutual coupling strength and the feedback strength in laser 2. When I_{SOA} is further increased to 39.00 mA [Figs. 5(e) and 5(f)], both lasers exhibit LFF dynamics, as can be seen in the increase of low-frequency components in the RF spectrum of Fig. 5(f).

We investigate the influence of the dynamics on the synchronization state of the high- and low-frequency components in each signal when the SOA injection current is changed. Figure 6 shows the temporal waveforms and the correlation plots between laser 1 and 2 at I_{SOA} = 6.00 mA for the original signals and the low-pass filtered signals at 1 GHz. The parameter values of Fig. 6 are the same as those of Figs. 5(a) and 5(b). We select the delay time τ of the cross correlation function C to maximize the absolute value of

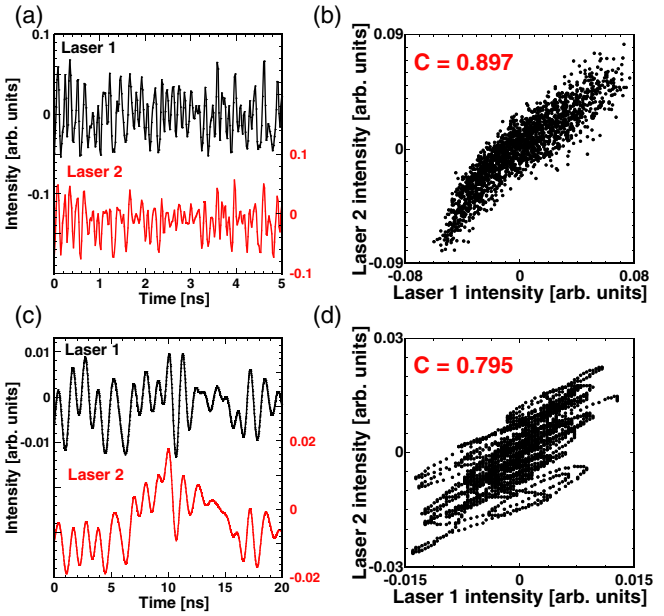

FIG. 6. Synchronization state at small SOA injection current I_{SOA} = 6.00 mA. (a, c) Temporal waveforms and (b, d) correlation plots. (a, b) Original signals and (c, d) low-pass filtered signals at f_c = 1 GHz. The parameter values correspond to those in Figs. 5(a) and 5(b).

C for each case, and sketch the corresponding correlation plots. First, when both lasers exhibit fast chaotic oscillations, in-phase synchronization is observed and high positive cross-correlation values are obtained between the original signals and between the filtered signals, as shown in Fig. 6.

Then, we increase the SOA injection current up to 25.00 mA and observe the temporal waveforms and correlation plots of the original and filtered signals, as shown in Fig. 7. The synchronization states show interesting changes. In-phase synchronization is observed for the original signals, while antiphase synchronization is observed for the filtered signals. The cross-correlation values are 0.739 and −0.523 for the original and filtered signals, respectively. In this case, laser 1 exhibits chaotic oscillations and laser 2 enters the LFF regime [see Figs. 5(c) and 5(d)]. We found that in-phase synchronization is observed between unfiltered high-frequency components and antiphase synchronization is observed between low-pass-filtered frequency components when one of the lasers shows chaotic oscillation and the other laser is in the LFF regime.

In Fig. 8, we further increase the SOA injection current up to 39.00 mA. In this case, the two lasers show LFF dynamics [Figs. 5(e) and 5(f)]. Antiphase synchronization is more clearly pronounced both between the original signals and between the filtered signals when both lasers show LFF dynamics.

In Fig. 9, we present the cross-correlation functions of the original and filtered signals. The peaks with the maximum absolute values in Figs. 9(a)–9(c) correspond to the correlation plots in Figs. 6–8, respectively. For the low SOA injection current (I_{SOA} = 6.00 mA) in Fig. 9(a), the peak interval of the cross-correlation function for the original signals corresponds to the inverse of the peak frequency of the chaotic oscillations (0.16 ns). The peaks of both the original and filtered signals

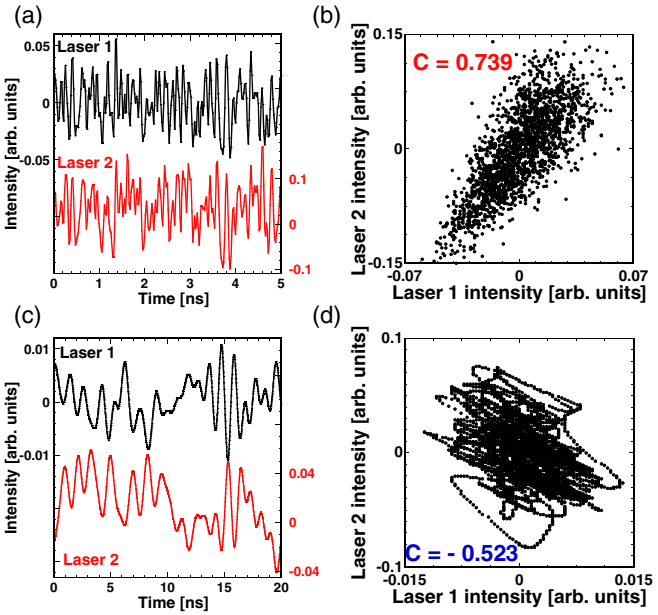

FIG. 7. Synchronization state at intermediate SOA injection current $I_{SOA} = 25.00$ mA. (a, c) Temporal waveforms and (b, d) correlation plots. (a, b) Original signals and (c, d) low-pass filtered signals at $f_c = 1$ GHz. The parameter values corresponds to Figs. 5(c) and 5(d).

show positive correlation values and in-phase synchronization is observed.

When the SOA injection current is increased to the intermediate value [$I_{SOA} = 25.00$ mA in Fig. 9(b)], the delay time corresponding to the peak of the cross-correlation function of the original signals does not change and in-phase

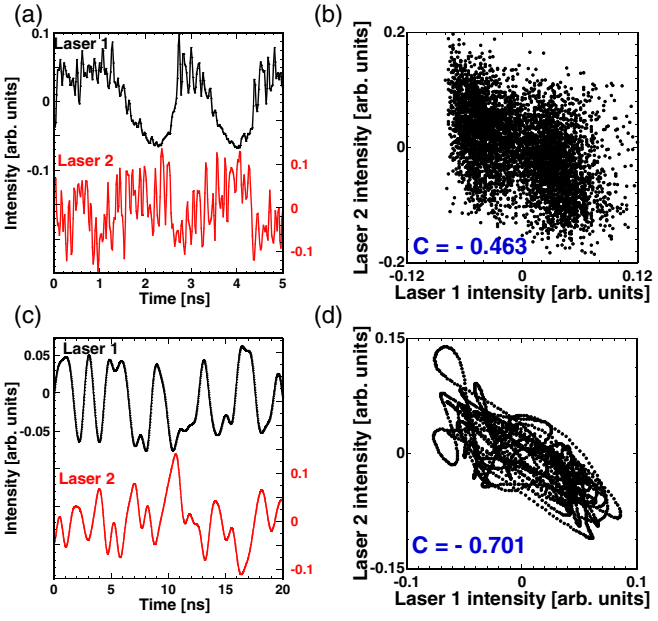

FIG. 8. Synchronization state at strong SOA injection current $I_{SOA} = 39.00$ mA. (a, c) Temporal waveforms and (b, d) correlation plots. (a, b) Original signals and (c, d) low-pass filtered signals at $f_c = 1$ GHz. The parameter values corresponds to Figs. 5(e) and 5(f).

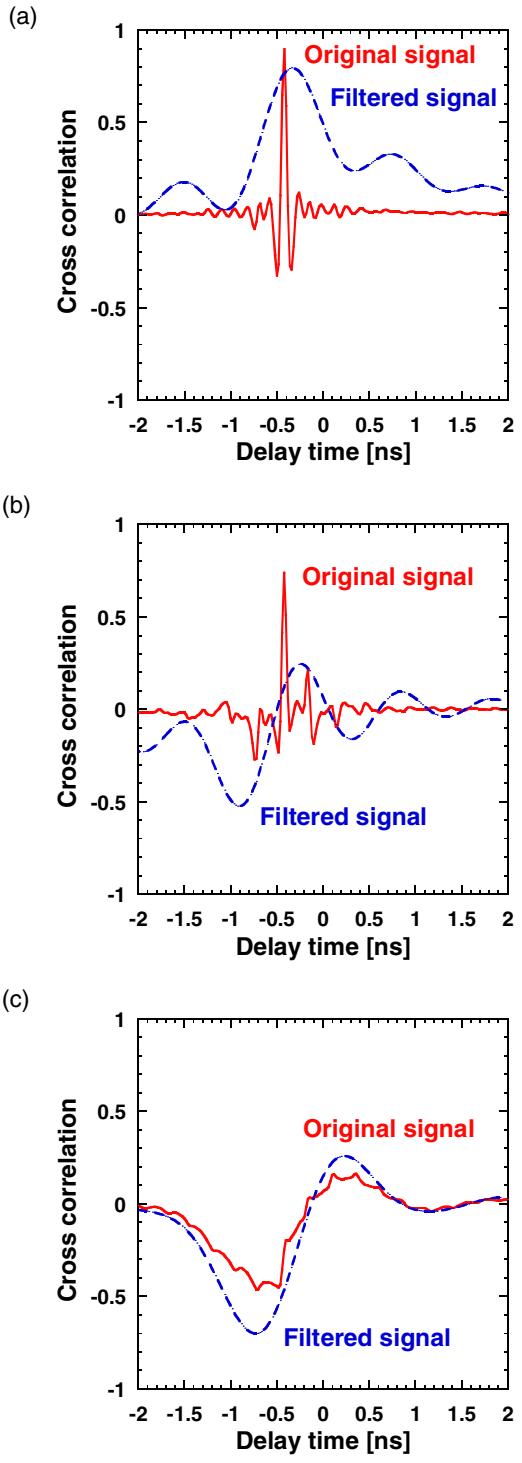

FIG. 9. Cross-correlation functions for the original signals (red solid line) and the low-pass filtered signals at 1 GHz (blue dashed line) of the two laser outputs for different SOA injection currents. (a) $I_{SOA} = 6.00$ mA, (b) $I_{SOA} = 25.00$ mA, and (c) $I_{SOA} = 39.00$ mA. (a, b, c) correspond to Figs. 6, 7, and 8, respectively. The correlation functions decay to zero when the lag time is over 5 ns (not shown).

synchronization is observed, similarly to Fig. 9(a). However, the correlation function for the filtered signal is completely re-shaped and a large negative peak appears at a different delay time. The maximum absolute value of the correlation function

for the filtered signals is −0.523. The correlation functions for the high and low frequency components in Fig. 9(b) look similar to those reported in systems showing episodic synchronization [25]. We will discuss the relationship between our observation and episodic synchronization in Sec. VI.

For the high SOA injection current [I_{SOA} = 39.00 mA in Fig. 9(c)], the peaks of the correlation function for both the original and filtered signals have negative values. The delay time at the peak of the correlation functions is shifted compared to its position in Fig. 9(a). We speculate that this shift is due to the occurrence of the LFF dynamics, as seen in Fig. 8. Therefore, the change in the synchronization state strongly depends on the change in the laser dynamics. We give the interpretation that the transition from chaos to LFF involves dynamical changes, introducing a new timescale corresponding to the irregular power dropouts visible in the time traces and characteristic of the LFF dynamics. This timescale is represented by the emergence of low-frequency components of relatively high amplitude in the spectra. The existence of this additional slow dynamics to the previous background of fast chaotic oscillations causes drastic changes in the synchronization properties between the lasers.

We discuss how the lag time of the correlation function changes with the change in the SOA injection current in Fig. 9. The chaotic waveform is re-shaped into LFF dynamics as the SOA injection current is increased. The lag time of the correlation is related to the fundamental time involved in the dynamics. For the original signal, a sharp peak appears in the correlation function at −0.4 ns in Fig. 9(a), indicating that laser 2 is leading laser 1. Besides, small peaks surrounding the high sharp peak are also observed. The time interval of the peaks corresponds to the average period of the chaotic oscillations. As the SOA injection current is increased, although the position of the peaks does not change, the position of the maximum peak is shifted to the next neighboring peak in the correlation function. These peaks in the correlation function disappear as the dynamics is shifted from chaos to LFF. For the high SOA current of Fig. 9(c), the LFF dynamics becomes dominant and the sharp peaks vanish. For the filtered signal, the lag time for the maximum correlation is continuously changed with the increase of the SOA injection current, and the peak interval of the correlation function roughly corresponds to the average period of the LFF power dropouts. This result indicates that the continuous change of the LFF dynamics can be interpreted in terms of evolution of the correlation function for the filtered signal.

V. RELATIONSHIP BETWEEN SYNCHRONIZATION AND DYNAMICS

We change the SOA injection current continuously to investigate the synchronization property for high and low frequency components. Figure 10 shows the evolution of the peak of the cross-correlation value for both the original and filtered signals when the SOA injection current I_{SOA} is changed and for the injection currents equal to $I_1/I_{th,1} = 1.5$ and $I_2/I_{th,2} = 3.5$. Figure 10 includes the results of Figs. 6, 7, and 8. We plotted the maximum of the absolute value of the cross-correlation function by changing the delay time τ for the calculation of C because the delay time corresponding to

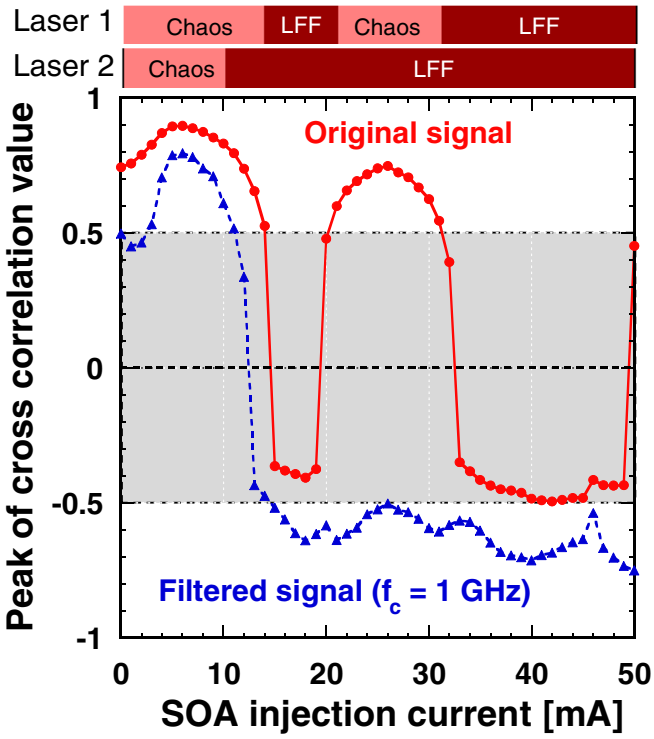

FIG. 10. Evolution of the cross-correlation value and dynamical states of the two lasers when the SOA injection current I_{SOA} is changed continuously for the original signals (red solid line with circles) and the low-pass filtered signals (blue dotted line with triangles). The gray region corresponds to loss of synchronization.

the peak value changes for different frequency components and different parameter values (see Fig. 9). The dynamics of each laser are also shown in the upper part of Fig. 10, and the change in I_{SOA} results in the change in the dynamics. We define in-phase and antiphase synchronization regions when $C \geqq 0.5$ and $C \leqq -0.5$, respectively. In addition, we define the region of loss of synchronization where the cross correlation value C ranges in $-0.5 < C < 0.5$ (the gray region in Fig. 10).

First, we discuss the influence of the laser dynamics on the synchronization state by changing I_{SOA}. Figure 10 shows that the synchronization state switches between in-phase and antiphase synchronization, as a result of the change in the laser dynamics. When chaotic dynamics are dominant in both lasers (0 mA $\leqq I_{SOA} \leqq$ 10 mA, see the upper part), in-phase synchronization is observed for both the original and the filtered signals. When LFF dynamics are dominant in both lasers (31 mA $< I_{SOA} \leqq$ 50 mA), antiphase synchronization is obtained for the filtered signals, while loss of synchronization with low negative correlation values is observed for the original signals. When LFF dynamics is dominant in laser 2 and coherence collapse chaos is exhibited in laser 1 (21 mA $\leqq I_{SOA} \leqq$ 31 mA), in-phase synchronization is observed for the original signals, while anti-phase synchronization is observed for the filtered signals. Therefore, we understand that the low-frequency components of LFF dynamics influence the synchronization properties. This fact reveals the dependence of the synchronization properties on the respective dynamics of the lasers.

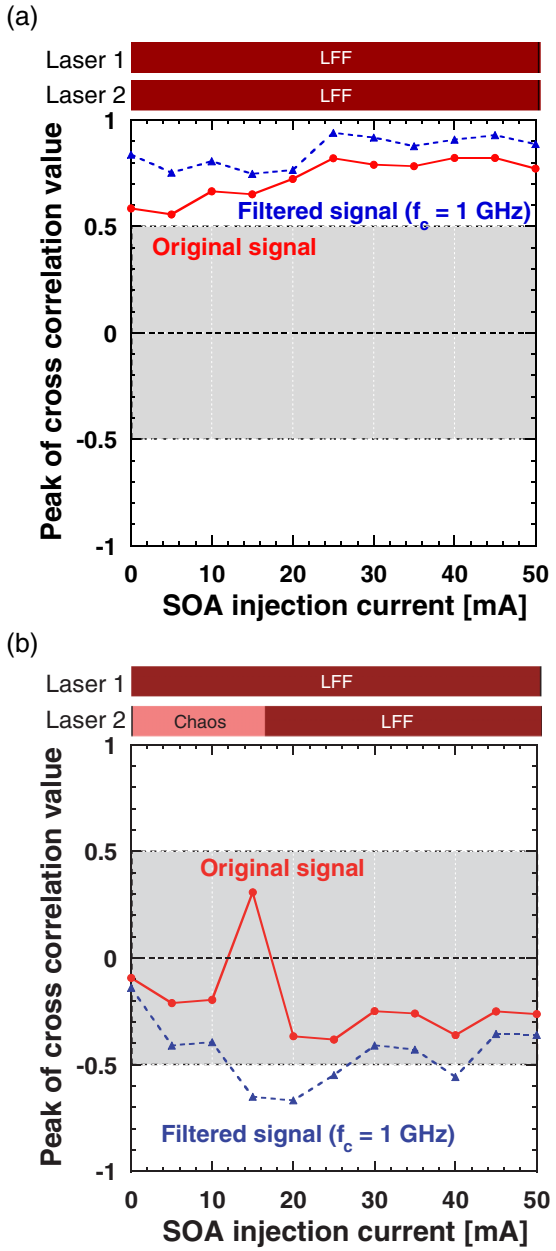

FIG. 11. Evolution of the cross-correlation value and dynamical states of the two lasers when the SOA injection current is changed continuously for the original signals (red solid line with circles) and the low-pass filtered signals (blue dotted line with triangles). We set different injection currents for laser 2: (a) $I_2/I_{\mathrm{th},2} = 5.0$ and (b) $I_2/I_{\mathrm{th},2} = 2.0$. The injection current for laser 1 is fixed at $I_1/I_{\mathrm{th},1} = 1.5$. The gray region corresponds to loss of synchronization.

Next, we investigate the evolution of the cross correlation for different injection currents in order to discuss the universality of the phenomenon shown Fig. 10. We only change the injection current in laser 2 ($I_2/I_{\mathrm{th},2}$), and we keep the injection current in laser 1 fixed ($I_1/I_{\mathrm{th},1} = 1.5$). In Fig. 11(a), when the injection current in laser 2 is large ($I_2/I_{\mathrm{th},2} = 5.0$), chaos synchronization is achieved and high cross correlation values are shown for all values of I_{SOA} for both the original and filtered signals. We found that high correlation can be achieved for very asymmetric injection currents. On the other hand, in Fig. 11(b), when $I_2/I_{\mathrm{th},2}$ is small ($I_2/I_{\mathrm{th},2} = 2.0$), synchronization is hardly observed and the cross correlation values are within the region of loss of synchronization for most parameter values.

We interpret that the balance of the injection currents of the two lasers is important to observe dynamics-dependent synchronization, as seen in Figs. 10 and 11. Synchronization is achieved when one of the lasers' injection current (and the optical injection power) is much larger than the other's [Fig. 11(a)]. However, loss of synchronization is found when the two lasers are driven with similar values of injection currents [Fig. 11(b)]. In the middle, dynamics-dependent synchronization can be observed in the transition from loss of synchronization to synchronization under intermediate coupling strength conditions (Fig. 10). We understand that in this system with mutually coupled lasers, the important parameters ruling the phenomenon of dynamics-dependent synchronization are the intermediate coupling strength, the asymmetric feedback strengths and the asymmetric injection currents.

VI. DISCUSSION

We discuss the fact that asymmetric system configurations and parameter settings are important to observe dynamics-dependent synchronization. In our PIC, both the coupling strength and the feedback strength in laser 2 are changed simultaneously when the SOA injection current is changed, while the feedback strength in laser 1 is always constant (see Fig. 1). The dynamics of laser 2 switches from chaos to LFF with the increase of the feedback strength, while laser 1 is kept in a chaotic state due to its fixed feedback strength. The coupling between these asymmetric dynamical behaviors induces a coexistence of in-phase and antiphase synchronization for high- (chaos) and low-frequency (LFF) components, respectively. This feature illustrates the fact that under intermediate coupling conditions, two dynamics of different nature can simultaneously induce in-phase and antiphase synchronization on distant frequency ranges. The experimental analysis reported here reveals the dynamical conditions under which these two types of synchronization coexist.

Another important feature is that we speculate that dynamics-dependent synchronization appears due to the temporal change in the optical frequency detuning between the two lasers. The analysis of temporal change in the optical frequency detuning has been carried out in coupled laser systems, as reported in Refs. [24,25] and known as episodic synchronization. Episodic synchronization is induced by the existence of LFF dynamics in which the locking of the optical frequencies are perturbed and short-term cross-correlation fluctuates in time [24]. The dynamical features presented here may suggest a phenomenon of episodic synchronization, since we found that the cross-correlation function of Fig. 9(b) resembles the results presented in Ref. [25].

The information provided in the optical spectra are also very valuable to understand the origin of dynamics-dependent synchronization. However, we cannot experimentally access the optical spectra of the lasers in our PIC, since it has no optical output port (see Fig. 1). Therefore, we will

numerically investigate the effects of the optical frequency detuning, asymmetric external cavity lengths and feedback strengths to analyze the mechanism of dynamics-dependent synchronization in our future work. In particular, we will numerically focus on the situation in which the optical coupling strength and the feedback strength in laser 2 are dependent, through a common and simultaneous amplification by the SOA, as it is the case in our experiment. We will also investigate the importance of short cavity configurations to observe dynamics-dependent synchronization.

VII. CONCLUSION

We investigated chaos synchronization in a photonic integrated circuit with two mutually-coupled semiconductor lasers. We applied a low-pass filter with the cut-off frequency of 1 GHz to the laser output signals in order to separate between low and high frequency components. We investigated the frequency dependence of chaos synchronization between the original and the low-pass-filtered signals. We observed in-phase synchronization between high-frequency components and anti-phase synchronization between low-frequency components, when one of the lasers shows chaotic oscillations while the other laser exhibits the LFF dynamics. This result reveals dynamics-dependent synchronization in mutually coupled lasers exhibiting different dynamical properties. Dynamics-dependent synchronization can be observed at intermediate coupling strengths with asymmetric feedback strengths and injection currents conditions, inducing different dynamical behaviors in the lasers. We consider that this phenomenon is universal and can be observed in a variety of asymmetrically coupled nonlinear dynamical systems.

PICs are promising technological devices for robust investigation of dynamics and chaos synchronization in coupled laser systems. The recent extension of the number of lasers on PICs is a promising technological tendency to observe more complex dynamics and different synchronization states in laser network systems [10–15], especially when short coupling timescales are involved.

ACKNOWLEDGMENTS

A.U. acknowledges support from Grants-in-Aid for Scientific Research from Japan Society for the Promotion of Science (JSPS KAKENHI Grant No. JP16H03878). The work was done while T. Harayama was at NTT Corporation.

[1] G. D. Van Wiggeren, and R. Roy, Communication with chaotic lasers, Science **279**, 1198 (1998).

[2] J.-P. Goedgebuer, L. Larger, and H. Porte, Optical Cryptosystem Based on Synchronization of Hyperchaos Generated by a Delayed Feedback Tunable Laser Diode, Phys. Rev. Lett. **80**, 2249 (1998).

[3] A. Argyris, D. Syvridis, L. Larger, V. Annovazzi-Lodi, P. Colet, I. Fischer, J. García-Ojalvo, C. R. Mirasso, L. Pesquera, and K. A. Shore, Chaos-based communications at high bit rates using commercial fibre-optic links, Nature **438**, 343 (2005).

[4] K. Yoshimura, J. Muramatsu, P. Davis, T. Harayama, H. Okumura, S. Morikatsu, H. Aida, and A. Uchida, Secure Key Distribution Using Correlated Randomness in Lasers Driven by Common Random Light, Phys. Rev. Lett. **108**, 070602 (2012).

[5] E. Klein, N. Gross, M. Rosenbluh, W. Kinzel, L. Khaykovich, and I. Kanter, Stable isochronal synchronization of mutually coupled chaotic lasers, Phys. Rev. E **73**, 066214 (2006).

[6] R. Vicente, C. R. Mirasso, and I. Fischer, Simultaneous bidirectional message transmission in a chaos-based communication scheme, Opt. Lett. **32**, 403 (2007).

[7] A. Uchida, *Optical Communication with Chaotic Lasers, Applications of Nonlinear Dynamics and Synchronization* (Wiley-VCH, Weinheim, 2012).

[8] J. Ohtsubo, *Semiconductor Lasers: Stability, Instability and Chaos*, 3rd ed. (Springer Verlag, Berlin, Heidelberg, 2013).

[9] B. B. Zhou and R. Roy, Isochronal synchrony and bidirectional communication with delay-coupled nonlinear oscillators, Phys. Rev. E **75**, 026205 (2007).

[10] B. Ravoori, A. B. Cohen, J. Sun, A. E. Motter, T. E. Murphy, and R. Roy, Robustness of Optimal Synchronization in Real Networks, Phys. Rev. Lett. **107**, 034102 (2011).

[11] J. Tiana-Alsina, K. Hicke, X. Porte, M. C. Soriano, M. C. Torrent, J. García-Ojalvo, and I. Fischer, Zero-lag synchronization and bubbling in delay-coupled lasers, Phys. Rev. E **85**, 026209 (2012).

[12] M. Nixon, M. Friedman, E. Ronen, A. A. Friesem, N. Davidson, and I. Kanter, Controlling Synchronization in Large Laser Networks, Phys. Rev. Lett. **108**, 214101 (2012).

[13] J. Ohtsubo, R. Ozawa, and M. Nanbu, Synchrony of small nonlinear networks in chaotic semiconductor lasers, Jpn. J. Appl. Phys. **54**, 072702 (2015).

[14] F. Böhm, A. Zakharova, E. Schöll, and K. Lüdge, Amplitude-phase coupling drives chimera states in globally coupled laser networks, Phys. Rev. E **91**, 040901 (2015).

[15] A. Argyris, M. Bourmpos, and D. Syvridis, Experimental synchrony of semiconductor lasers in coupled networks, Opt. Express **24**, 5600 (2016).

[16] T. Sano, Antimode dynamics and chaotic itinerancy in the coherence collapse of semiconductor lasers with optical feedback, Phys. Rev. A **50**, 2719 (1994).

[17] I. Fischer, G. H. M. van Tartwijk, A. M. Levine, W. Elsäßer, E. Göbel, and D. Lenstra, Fast Pulsing and Chaotic Itinerancy with a Drift in the Coherence Collapse of Semiconductor Lasers, Phys. Rev. Lett. **76**, 220 (1996).

[18] M. Sciamanna, A. Tabaka, H. Thienpont, and K. Panajotov, Intensity behavior underlying pulse packages in semiconductor lasers that are subject to optical feedback, J. Opt. Soc. Am. B **22**, 777 (2005).

[19] W. Ray, W.-S. Lam, P. N. Guzdar, and R. Roy, Observation of chaotic itinerancy in the light and carrier dynamics of a semiconductor laser with optical feedback, Phys. Rev. E **73**, 026219 (2006).

[20] D. Brunner, M. C. Soriano, X. Porte, and I. Fischer, Experimental Phase-Space Tomography of Semiconductor Laser Dynamics, Phys. Rev. Lett. **115**, 053901 (2015).

[21] T. Heil, I. Fischer, W. Elsäßer, J. Mulet, and C. R. Mirasso, Chaos Synchronization and Spontaneous Symmetry-Breaking

in Symmetrically Delay-Coupled Semiconductor Lasers, Phys. Rev. Lett. **86**, 795 (2001).

[22] M. Ozaki, H. Someya, T. Mihara, A. Uchida, S. Yoshimori, K. Panajotov, M. Sciamanna, Leader-laggard relationship of chaos synchronization in mutually coupled vertical-cavity surface-emitting lasers with time delay, Phys. Rev. E **79**, 026210 (2009).

[23] I. Wedekind and U. Parlitz, Chaos synchronization and spontaneous symmetry-breaking in symmetrically delay-coupled semiconductor lasers, Int. J. Bifurcat. Chaos **11**, 1141 (2001)

[24] J. M. Buldú, T. Heil, I. Fischer, M. C. Torrent, and J. García-Ojalvo, Episodic Synchronization via Dynamic Injection, Phys. Rev. Lett. **96**, 024102 (2006).

[25] J. F. M. Ávila, R. Vicente, J. R. R. Leite, and C. R. Mirasso, Synchronization properties of bidirectionally coupled semiconductor lasers under asymmetric operating conditions, Phys. Rev. E **75**, 066202 (2007).

[26] K. Hicke, O. D'Huys, V. Flunkert, E. Schöll, J. Danckaert, and I. Fischer, Mismatch and synchronization: Influence of asymmetries in systems of two delay-coupled lasers, Phys. Rev. E **83**, 056211 (2011).

[27] M. Peil, L. Larger, and I. Fischer, Versatile and robust chaos synchronization phenomena imposed by delayed shared feedback coupling, Phys. Rev. E **76**, 045201(R) (2007).

[28] T. Heil, I. Fischer, W. Elsäßer, and A. Gavrielides, Dynamics of Semiconductor Lasers Subject to Delayed Optical Feedback: The Short Cavity Regime, Phys. Rev. Lett. **87**, 243901 (2001).

[29] T. Heil, I. Fischer, W. Elsäßer, B. Krauskopf, K. Green, and A. Gavrielides, Delay dynamics of semiconductor lasers with short external cavities: Bifurcation scenarios and mechanisms, Phys. Rev. E **67**, 066214 (2003).

[30] A. Argyris, M. Hamacher, K. E. Chlouverakis, A. Bogris, and D. Syvridis, Photonic Integrated Device for Chaos Applications in Communications, Phys. Rev. Lett. **100**, 194101 (2008).

[31] A. Karsaklian Dal Bosco, K. Kanno, A. Uchida, M. Sciamanna, T. Harayama, and K. Yoshimura, Cycles of self-pulsations in a photonic integrated circuit, Phys. Rev. E **92**, 062905 (2015).

[32] J. P. Toomey, D. M. Kane, C. McMahon, A. Argyris, and D. Syvridis, Integrated semiconductor laser with optical feedback: Transition from short to long cavity regime, Opt. Express **23**, 18754 (2015).

[33] A. Karsaklian Dal Bosco, Y. Akizawa, K. Kanno, A. Uchida, T. Harayama, and K. Yoshimura, Photonic integrated circuits unveil crisis-induced intermittency, Opt. Express **24**, 22198 (2016).

[34] A. Argyris, S. Deligiannidis, E. Pikasis, A. Bogris, and D. Syvridis, Implementation of 140 Gb/s true random bit generator based on a chaotic photonic integrated circuit, Opt. Express **18**, 18763 (2010).

[35] T. Harayama, S. Sunada, K. Yoshimura, P. Davis, K. Tsuzuki, and A. Uchida, Fast nondeterministic random-bit generation using on-chip chaos lasers, Phys. Rev. A **83**, 031803(R) (2011).

[36] R. Takahashi, Y. Akizawa, A. Uchida, T. Harayama, K. Tsuzuki, S. Sunada, K. Arai, K. Yoshimura, and P. Davis, Fast physical random bit generation with photonic integrated circuits with different external cavity lengths for chaos generation, Opt. Express **22**, 11727 (2014).

[37] H.-J. Wünsche, S. Bauer, J. Kreissl, O. Ushakov, N. Korneyev, F. Henneberger, E. Wille, H. Erzgräber, M. Peil, W. Elsäßer, and I. Fischer, Synchronization of Delay-Coupled Oscillators: A Study of Semiconductor Lasers, Phys. Rev. Lett. **94**, 163901 (2005).